1 K for Miranda and Ariel, respectively. From the relation $A = 1 - R^2(T_{ss}/T_0)^4$ (where A is the local albedo), the bolometric albedos in the south polar regions of the two objects are therefore 0.23 ± 0.06 and 0.30 ± 0.05, respectively. Here, R is the distance from Uranus to the sun [19.122 astronomical units (AU)], and the radiative properties of the satellites are assumed to be uniform. T_0, the subsolar point equilibrium temperature for 0° phase angle at 1 AU, would be 395 K for a Lambertian surface. However, peaking of the infrared emission at low phase angles leads to an observed value of 400 K for Earth's moon (*16*), while observations of other satellites and of asteroids suggest values as high as 408 K. For the present calculations, we adopt 401 ± 6 K for T_0.

To determine the Bond albedos (A_B) from the local albedos (A) requires knowledge of the surface phase function. On the basis of a surface-scattering model, Goguen (*17*) estimates that for two extreme cases of surface microstructure—strongly backscattering, low-albedo grains and isotropically scattering, high-albedo grains—A_B/A varies from 1.0 to 1.1. Adopting the mean value and associated uncertainty leads to a bolometric A_B of 0.24 ± 0.06 for Miranda and of 0.31 ± 0.06 for Ariel.

From ground-based photometry, the visual magnitudes $V(1,0)$ of Miranda and Ariel are 3.79 ± 0.17 and 1.48 ± 0.15, respectively (*18*). Combining these values with the newly determined radii of 242 ± 5 and 580 ± 5 km (*14*) yields geometric albedos (p_v) of 0.23 ± 0.04 and 0.33 ± 0.05. Where existing data sets overlap, the visible and near-infrared disk spectra of Ariel and Rhea are similar (*19*). From the Rhea data, we determined that the bolometric geometric albedo (p_B) of Rhea, normalized to its reflectivity at 0.56 μm, is 0.89. By assuming that this value is also representative of Miranda and Ariel, p_B (derived from p_v) is 0.20 ± 0.04 for Miranda and 0.30 ± 0.04 for Ariel; we have included an additional 5% uncertainty to allow for spectral differences between Rhea and the Uranian satellites. The phase integrals, equal to A_B/p_B, are therefore 1.17 ± 0.37 and 1.05 ± 0.25, respectively. These values are higher than expected for objects of relatively low albedo (*20*) and suggest a different surface microstructure, such as one composed of dark, relatively isotropically scattering grains (*17*).

REFERENCES AND NOTES

1. R. Hanel *et al.*, *Appl. Opt.* **19**, 1391 (1980).
2. R. Hanel, in *Spectrometric Techniques*, G. Vanasse, Ed. (Academic Press, New York, 1983), vol. 3, chap. 2.
3. G. Birnbaum and E. R. Cohen, *Can. J. Phys.* **54**, 593 (1976); E. R. Cohen and G. Birnbaum, *Natl. Bur. Stand. Intern. Rep. 80-2175* (1981); P. Dore, L. Nencini, G. Birnbaum, *J. Quant. Spectrosc. Rad. Transfer* **30**, 245 (1983); G. Bachet, E. R. Cohen, P. Dore, G. Birnbaum, *Can. J. Phys.* **61**, 591 (1983).
4. G. S. Orton, *Science* **231**, 836 (1986).
5. D. Gautier *et al.*, *J. Geophys. Res.* **86**, 8713 (1981).
6. B. Conrath, D. Gautier, R. Hanel, J. S. Hornstein, *Astrophys. J.* **282**, 807 (1984).
7. G. Lindal, personal communication; G. L. Tyler *et al.*, *Science* **233**, 79 (1986).
8. Y. Lebreton and A. Maeder, *Astron. Astrophys.*, in press; M. Casse, S. Cahen, C. Doom, *Proceedings of the Colloquium of the French Physical Society*, Nice, France, 9–13 September 1985.
9. A. Noels, R. Scuflaire, M. Gabriel, *Astron. Astrophys.* **130**, 389 (1984).
10. G. Orton *et al.*, *Icarus*, in press.
11. S. H. Moseley, B. J. Conrath, R. Silverberg, *Astrophys. J.* **292**, L83 (1985).
12. L. Wallace, *Icarus* **54**, 110 (1983); B. Bezard and D. Gautier, *Proceedings of the Conference on the Jovian Atmospheres*, New York, NY, 6–8 May 1985; J. Appleby, *Icarus*, in press.
13. J. R. Holton, *An Introduction to Dynamic Meteorology* (Academic Press, New York, 1979).
14. B. A. Smith *et al.*, *Science* **233**, 43 (1986).
15. J. Pirraglia, B. Conrath, M. Allison, P. Gierasch, *Nature (London)* **292**, 677 (1981).
16. J. Saari, R. Shorthill, D. Winter, *Moon* **5**, 179 (1972).
17. J. Goguen, personal communication; *Bull. Am. Astron. Soc.* **17**, 728 (1985).
18. D. P. Cruikshank, in *Uranus and the Outer Planets*, G. Hunt Ed. (Cambridge Univ. Press, Cambridge, England, 1982), p. 193.
19. R. N. Clark and P. D. Owensby, *Icarus* **46**, 354 (1981); R. H. Brown, *ibid.* **56**, 414 (1983).
20. R. Hanel *et al.*, *Science* **215**, 544 (1982).

21. We thank G. F. Lindal and G. L. Tyler of the radio science team for providing temperature profiles before publication; A. L. Lane for making computing facilities available to us; A. Ingersoll for many valuable comments; V. Suomi and R. Beebe for useful discussions; G. Orton for providing us with Fortran code for CH_4–H_2 absorption coefficients; and S. Akula, S. Bahethi, A. Gabbay, J. Guerber, L. Herath, P. Manava, L. Mayo, W. Shaffer, M. Silverstein, and J. Tingley for computer programming support.

31 March 1986; accepted 5 May 1986

Ultraviolet Spectrometer Observations of Uranus

A. L. BROADFOOT, F. HERBERT, J. B. HOLBERG, D. M. HUNTEN, S. KUMAR, B. R. SANDEL, D. E. SHEMANSKY, G. R. SMITH, R. V. YELLE, D. F. STROBEL, H. W. MOOS, T. M. DONAHUE, S. K. ATREYA, J. L. BERTAUX, J. E. BLAMONT, J. C. MCCONNELL, A. J. DESSLER, S. LINICK, R. SPRINGER

Data from solar and stellar occultations of Uranus indicate a temperature of about 750 kelvins in the upper levels of the atmosphere (composed mostly of atomic and molecular hydrogen) and define the distributions of methane and acetylene in the lower levels. The ultraviolet spectrum of the sunlit hemisphere is dominated by emissions from atomic and molecular hydrogen, which are known as electroglow emissions. The energy source for these emissions is unknown, but the spectrum implies excitation by low-energy electrons (modeled with a 3-electron-volt Maxwellian energy distribution). The major energy sink for the electrons is dissociation of molecular hydrogen, producing hydrogen atoms at a rate of 10^{29} per second. Approximately half the atoms have energies higher than the escape energy. The high temperature of the atmosphere, the small size of Uranus, and the number density of hydrogen atoms in the thermosphere imply an extensive thermal hydrogen corona that reduces the orbital lifetime of ring particles and biases the size distribution toward larger particles. This corona is augmented by the nonthermal hydrogen atoms associated with the electroglow. An aurora near the magnetic pole in the dark hemisphere arises from excitation of molecular hydrogen at the level where its vertical column abundance is about 10^{20} per square centimeter with input power comparable to that of the sunlit electroglow (approximately 2×10^{11} watts). An initial estimate of the acetylene volume mixing ratio, as judged from measurements of the far ultraviolet albedo, is about 2×10^{-7} at a vertical column abundance of molecular hydrogen of 10^{23} per square centimeter (pressure, approximately 0.3 millibar). Carbon emissions from the Uranian atmosphere were also detected.

THE VOYAGER ULTRAVIOLET SPECTROMETER (UVS), an objective-grating instrument, detects wavelengths from approximately 500 to 1700 Å by means of 126 contiguous channels and has a field of view 0°.1 by 0°.86.

Temperature and composition of the upper atmosphere. We measured the transmission of the Uranian atmosphere over 6000 km of altitude by recording light from the stars γ Pegasi and ν Geminorum and from the sun as each was occulted by Uranus' atmosphere (Table 1). When referred to a common geopotential (*1*), the occultations of the sun and γ Pegasi show similar transmission profiles at latitudes near 0° and near the light and dark poles, except for possible differences in the hydrocarbon profiles of up to one scale height.

Figure 1 shows light curves for three key wavelength regions (*2*). Continuum absorption by H_2 at wavelengths less than 845 Å (panel A) probes the highest levels; this range is accessible only in the solar occulta-

tion because starlight of wavelength less than 912 Å is absorbed by interstellar H. All occultations measured absorption in the discrete transitions of the H_2 Rydberg systems. This absorption is about 10^3 times weaker than the continuum absorption and probes lower altitudes in the strong line region of the curve of growth (panel B). The interpretation of this light curve is based on models of the band absorption, which compare favorably with measurements of interstellar H_2 absorption made by the satellite OAO-3 *Copernicus* (*3*). Agreement is better than a factor of 2 for H_2 column densities in the range of interest here. The model points compared with the data in Fig. 1, A and B, were computed from the altitude profiles in Fig. 2, which include a temperature of 750 K at altitudes higher than 27,700 km. The match to the individual shapes of the light curves in Fig. 1, A and B, is evidence that the profile is accurate, but the locations of the temperature changes are not uniquely determined. A more sensitive verification of the model's temperature is that its H_2 profile is consistent with the measured altitude difference between the half-light points in Fig. 1, A and B. These points represent two levels in the atmosphere having H_2 densities that differ by a factor of about 2×10^4, corresponding to about ten scale heights.

The abundance of atomic hydrogen can best be inferred from absorption at wavelengths between 845 and 912 Å, where H absorbs in its ionization continuum. Discrete H_2 absorption in this region must be corrected for by using the H_2 profile. This procedure yields an H density of 1×10^8 cm^{-3} at a distance of 27,930 km from Uranus center. Extrapolating this density to the orbital distance of the rings implies the existence of substantial H number densities that influence ring evolution through gas drag.

Absorption by CH_4 causes the abrupt drop in transmission at approximately 25,950 km from Uranus center (Fig. 1C). The absorption signature of C_2H_2 appears near this altitude as well (*4*). The scale heights are 30 to 35 km for CH_4 (Fig. 2) and 25 to 30 km for C_2H_2. Near the half-light points, the data are matched by a model in which the ratio $[C_2H_2]:[CH_4]$ is approximately 0.3. Initial photochemical models indicate that this ratio is reached at atmospheric pressures of 3 to 10 μbar (*5*). The hydrocarbon distributions in this region are probably determined by diffusion and photochemical processes rather than by hydrostatic equilibrium. The scale heights therefore cannot be interpreted directly in terms of a temperature. Earth-based observations of stellar occultations (*6*) imply a temperature between 120 and 155 K in this region, which is below the hotter thermosphere. The corresponding H_2 scale height is consistent with our observations.

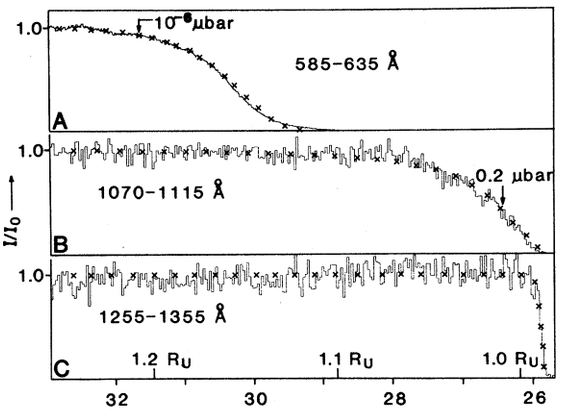

Fig. 1. Light curves measured in the occultation observations. The abscissa is distance measured from the center of the planet ($\times 10^3$ km) referred to a common geopotential at the equator. The model fits (X) were computed from the altitude profiles in Fig. 2. (A) Solar occultation, H_2 continuum; (B) γ Pegasi occultation, H_2 band absorption; (C) γ Pegasi occultation, CH_4 absorption.

Extreme ultraviolet (EUV) emission from the sunlit atmosphere. The EUV emission spectrum of Uranus' sunlit atmosphere contains particle-excited discrete and continuum radiation from H_2, HI Rydberg series emission, solar reflection continuum radiation at wavelengths greater than 1500 Å, and discrete features corresponding to transitions in CI and possibly other species. A spectrum obtained near the subsolar point is shown in Fig. 3; the only easily measurable feature in the dark atmosphere spectrum is a weak H Lyman α line. This difference in EUV emission between sunlit and dark atmospheres is similar to what was observed at Jupiter and Saturn (*7*, *8*). The energy deposited in the sunlit atmosphere is large, and the mechanism is unexplained (*9–11*); solar radiation appears to be required as a stimulus. The emission is more or less uniformly distributed over the sunlit hemisphere and shows no direct dependence on magnetic field strength or populations of trapped particles (*11*). Although there are planet-to-planet differences in the phenomenon, the energy in each case is sufficient to control the high-altitude temperature, atmospheric composition, and ionospheres of the three planets (*9–11*). These emissions are distinct from dayglow and aurora, and we suggest the name "electroglow" for them. A similar phenomenon has been observed at Titan, but its energy source may be precipitation from Saturn's magnetosphere (*12*).

Molecular and atomic hydrogen emissions. Figure 3 shows the spectrum of Uranus compared to an equatorial subsolar spectrum of Saturn. The major difference between the spectra is in the larger amount of energy longward of 1100 Å in the Uranus spectrum. Approximately 80% of the particle-excited emission from Uranus is in the wavelength range longward of the H Lyman α line. These long wavelength emissions, which are not found in the spectra of Saturn

Table 1. UVS occultation observations.

Star	Resolution		Latitude (degrees)	Range (R_U)	Time relative to encounter (hours)	Comments
	Height (km)	Radial (km)				
			Atmosphere			
γ Pegasi	5.7		+66		−0.5	Entrance, radial
γ Pegasi	5.7		−69		+0.5	Exit, radial
ν Geminorum*	<3.8		+4		+6.0	Grazing
Sun	2.6		+4		+2.0	Entrance, radial
			Rings			
σ Sagittarii		<0.3		2.0–1.8	−12	ε and δ rings
β Persei		3		2.0	+1.5	High magnetospheric background

*Analysis of ν Geminorum observation is in progress.

A. L. Broadfoot, F. Herbert, J. B. Holberg, D. M. Hunten, S. Kumar, B. R. Sandel, D. E. Shemansky, G. R. Smith, R. V. Yelle, Lunar and Planetary Laboratory, University of Arizona, Tucson, AZ 85721.
D. F. Strobel and H. W. Moos, Department of Physics, Johns Hopkins University, Baltimore, MD 21218.
T. M. Donahue and S. K. Atreya, Department of Atmospheric and Oceanic Science, University of Michigan, Ann Arbor, MI 48109.
J. L. Bertaux and J. E. Blamont, Service d'Aeronomie du Centre National de la Recherche Scientifique, B.P.N. 3 91370 Verrieres le Buisson, France.
J. C. McConnell, Department of Earth and Atmospheric Sciences, York University, Downsview, Toronto, M3J 1P3 Canada.
A. J. Dessler, Space Science Laboratory, Marshall Space Flight Center, Huntsville, AL 35812.
S. Linick and R. Springer, Jet Propulsion Laboratory, California Institute of Technology, Pasadena, CA 91109.

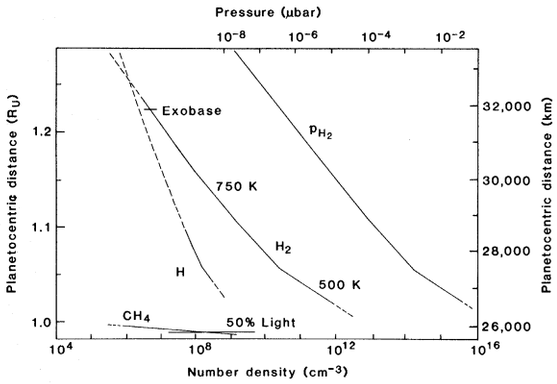

Fig. 2. The atmospheric profile that best reproduces the occultation light curves. Here we take 1 R_U = 26,200 km. The H_2 distribution was measured over the indicated altitude range. The model profiles were calculated on the assumption of diffusive separation and hydrostatic equilibrium in three layers of constant temperature. Layer boundaries, density scale factors, and temperatures were varied to find the best fit to the measured light curves. The dashed portion of the H profile is an extrapolation of the number density measured near 1.1 R_U based on the temperature inferred from the H_2 profile. The CH_4 profile that best models the observations is shown near its 50% transmission level, where its (probably height-dependent) scale height was measured. Near this level, the ratio $[C_2H_2]$:$[CH_4]$ is approximately 0.3. Absorption by helium is masked by the more abundant H_2, but resonance scattering from He at 584 Å has been detected from the atmosphere.

or Jupiter, must be attributed to H_2 continuum transitions. Model calculations used in the analysis of the spectra (*10*) on Jupiter and Saturn have been expanded to include the H_2 ($a\ ^3\Sigma_g^+$ to $b\ ^3\Sigma_u^+$) continuum (denoted H_2 *a–b*) (*13*). The H_2 *a–b* continuum is excited efficiently only by low-energy electrons. The spectrum in Fig. 3 requires a model calculated at an electron temperature T_e of approximately 3 eV to obtain the proper proportion of continuum radiation. Saturn and Jupiter electroglow spectra are modeled with T_e in the range from 30 to 60 eV (*10*, *14*, *15*). Consequently, the branching of electron energy deposition is quite different on Uranus. The results of a an initial analysis are given in Table 2, with comparative values for Saturn. Significant aspects of the atmospheric excitation process are as follows.

1) The total production rate for H at Uranus is comparable to that at Saturn, although the energy deposition flux is lower (Table 2). The mean emission altitude occurs at vertical column abundances of about 10^{15} cm^{-2} in H_2 and 3×10^{14} cm^{-2} in H (*16*) ($[H]$:$[H_2]$ ~0.15); these abundances are comparable to those on Saturn and Jupiter. Extrapolating the H density measured in the occultation data to the atmospheric level corresponding to 10^{15} cm^{-2} column abundance in H_2 yields an $[H]$:$[H_2]$ ratio of 0.2. If the emissions do arise above the exobase, a large fraction of the H can escape into the magnetosphere (*11*).

2) The energy flux (0.08 erg cm^{-2} sec^{-1}) deposited in the sunlit atmosphere is sufficient to explain the high exospheric neutral temperature of about 750 K; 75% of the energy flux is deposited in direct dissociation and dissociative excitation (*11*). The branching of energy in this calculation depends on the assumption that most of the H_2 is in the $v = 0$ vibrational level. The large cross section for vibrational excitation by electrons, especially for the $v = 1$ level, will alter the rates and branching of energy deposition. This is a nonlinear system not easily predicted without detailed modeling.

3) The atmospheric ionization rate is small compared to the neutral excitation rate (Table 2).

4) The low mean energy of the exciting electrons argues against precipitating particles as direct contributors to the atmospheric excitation (*17*, *18*).

Figure 4 shows that the electroglow emissions are relatively uniform over the sunlit disk except for strong peaks near the bright limb in H Lyman α and H_2 (Lyman + Werner) emissions at short wavelengths; the H Lyman α peak is the broader of the two. The band from 1273 to 1523 Å, corresponding to H_2 Lyman and H_2 *a–b* emissions, generally follows the short wavelength H_2 (Lyman + Werner) emissions but shows no peak at the limb. The spectrum from the peaks suggests high-altitude excitation of H and H_2 by electrons having higher energy than those near the center of the disk (characteristic temperature ≳30 eV). The morphology of the electroglow is different on Jupiter, Saturn, and Uranus (*10*, *19*).

Hydrogen Lyman α and H_2 emissions—altitude profiles. By means of two bright-limb drifts, at 6 and 2 hours before Uranus encounter, the UVS measured the altitude profile of the EUV emissions; the two drifts sampled the limb at latitudes of 45° and near the sunlit pole, respectively. Figure 5 shows the altitude profiles of H Lyman α and H_2 band emissions inferred from the drift 2 hours before encounter. Both emissions peak at approximately 27,350 km from Uranus center, but the H_2 band emissions appear to extend to somewhat higher altitudes. According to the occultation results, continuous absorption is negligible at these wavelengths in this altitude range; thus the decrease in intensity at lower altitudes reflects a real decrease in emissivity.

The peak in H Lyman α emission is surprising because it suggests an internal, optically thin source, whereas emission from a thermal source would be optically thick at the column abundances appropriate for the limb drifts. Similar behavior observed on Saturn led Yelle and colleagues (*19*) to argue that this brightening is evidence for precipitating protons or fast H atoms. Because the H:H_2 mixing ratio is small at the altitude represented by the peak, the emissions probably result from the excitation of the energetic protons or H atoms as they impact H_2. Dissociative excitation of H_2 may produce H Lyman α emissions, but the intensity from this source is constrained to less than

Table 2. Upper-atmospheric emission and energy deposition on Saturn and Uranus.

Emission or energy deposition	Saturn	Uranus
	Electroglow	
$I(H_2$ Lyman), subsolar	530 Ry	360 Ry
$I(H_2$ Werner), subsolar	440 Ry	35 Ry
$I(H_2$ *a–b*), subsolar	~60 Ry	1400 Ry
$I(H_2$ Lyman α), subsolar*	3500 Ry†	1500 Ry
Solar reflection continuum (1600 Å), subsolar	13.0 Ry Å^{-1}	6.5 Ry Å^{-1}
Geometric albedo (1600 Å), subsolar‡	0.23	0.45
e + H_2 → 2H	1.7×10^9 cm^{-2} sec^{-1}§	5.5×10^9 cm^{-2} sec^{-1}
e + H_2 → 2H	1.5×10^{29} sec^{-1}§	1.2×10^{29} sec^{-1}
e + H_2 → H_2^+, H^+	10^9 cm^{-2} sec^{-1}	0.2×10^9 cm^{-2} sec^{-1}
Deposition energy rate, uniform disk	0.13 erg cm^{-2} sec^{-1}	0.08 erg cm^{-2} sec^{-1}
Total power input	1.5×10^{12} W	0.17×10^{12} W
Solar ionizing radiation	0.016 erg cm^{-2} sec^{-1}	0.004 erg cm^{-2} sec^{-1}
Solar wind flux	0.005 erg cm^{-2} sec^{-1}	0.001 erg cm^{-2} sec^{-1}
	Aurora	
$I(H_2$ Ly + Wr)‖	~10 kRy	9 kRy
I(H Lyman α)‖	~20 kRy	1.5 kRy
Deposition energy rate, uniform disk	0.4×10^{12} W	0.2×10^{12} W

*Total rate, including resonance scattering. †Data from Voyager 2 encounter. ‡$\pi F = 1.33 \times 10^9$ photon cm^{-2} sec^{-1}. §Data from (*11*). ‖See text for disk averages.

200 Ry by the measured H_2 band intensity. Therefore an additional source of H Lyman α that produces optically thin radiation is required; energetic protons or H atoms are possibilities.

The H_2 emissions peak at nearly the same altitude in both drifts, as do the H Lyman α emissions. The H Lyman α intensity is 10% to 20% smaller in the drift at 6 hours before encounter, but the H_2 band intensity is 10% to 20% larger. This indicates a change in the distribution of exciting particles with latitude or excitation at different levels and consequently at different [H]:[H_2] ratios.

The H_2 emissions shown in Fig. 5 peak well below the exobase and fall sharply at altitudes above 1.1 Uranus radii (R_U). The spectral analysis, on the other hand, implies an average excitation altitude near the exobase, at 1.2 R_U. A more detailed study is required to determine the altitude variation of the volume emission rate from the limb profiles, but we note that low-intensity H_2 emissions extending to several R_U would shift the average excitation to higher altitudes. This may be the case because the H_2 emissions seen on the limb cannot account for the intensity seen in the downward-looking observations. A rough estimate indicates that the limb observations, when corrected to the zenith, can account for only 30% of the disk intensity. This implies that most of the H_2 emissions occur at higher altitudes or that there is significantly more absorption in the limb spectra than in the subsolar spectra.

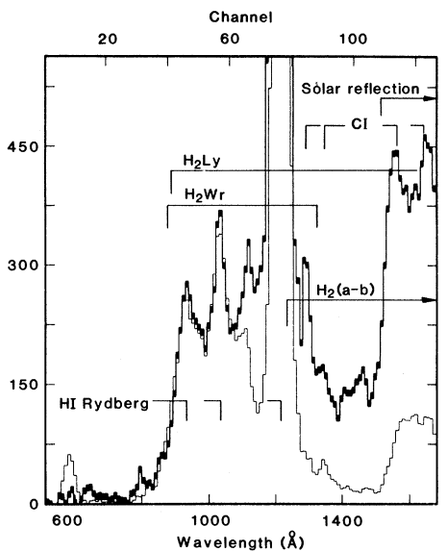

Fig. 3. Spectra of the electroglow emissions on Uranus and Saturn. The ordinate is in units of counts per 3840 seconds. Heavy line: Uranus spectrum near the subsolar point obtained on 23 January 1986 universal time (U.T.); integration time, 137,355 seconds. Light line: Voyager 2 Saturn spectrum obtained on 24 August 1981 U.T., in the subsolar equatorial region. The Saturn spectrum is normalized to the Uranus emission in the short wavelength H_2 band region. The H Lyman α line peaks off the scale (see Table 1 and text for quantitative data).

Table 3. Hydrogen Lyman α emission intensity as a function of distance in the Uranian system.

Distance (R_U)	Intensity (Ry)		
	Measured	Background	Coronal
1.5	500	350	150
2.0	390	290	100
3.8	350	290	60
50*	290	290	0

*This measurement is assumed to represent the background.

Other observations support the idea of an extended H distribution in the Uranus system. Table 3 shows that the H Lyman α intensity off the disk decreases with distance but remains significantly above the interstellar medium background for distances up to several R_U. Resonant scattering of solar, interstellar medium, and planetary H Lyman α emissions by the thermal exosphere inferred from the occultation analysis (Fig. 6) cannot account for the measured intensity. This implies additional H excitation or a nonthermal distribution of H in addition to the 750 K exosphere.

Exospheric drag and ring evolution. The extended Uranian exosphere influences the dynamical evolution of the rings. Even in the absence of collisions, the inner part of an exosphere should be in solid-body rotation (*20*), a result verified by our own numerical calculations. The reduction of effective gravity toward the equatorial plane because of planetary spin also increases the scale height and therefore the density at high altitudes. In the region of the rings (1.6 to 2 R_U), this model is well fitted by the extrapolation expression

$$n_H = 7 \times 10^{-6}\, e^{32.4/r} \mathrm{cm}^{-3} \qquad (1)$$

where r is in units of the planetary radius (26,200 km); n_H is normalized to our occultation value at 27,930 km. The drag force can be expressed as $D = C_D\, A_p\, \rho\, V_{rel}^2$ for a ring particle moving with relative velocity V_{rel} through a gas of density ρ. Here C_D is the drag coefficient, usually near unity, and A_p is the mean cross-sectional area of the particle. Equating the drag torque to the loss of angular momentum of an orbiting particle, we can derive the decay rate of the orbit. For a ring particle of mass M_p in a circular orbit in a hydrogen exosphere of number density in n_H, this rate is given by

$$dr/dt = -2\, C_D\, (A_p/M_p)\, n_H\, m_H\, r\, V_{rel}^2/V_o \qquad (2)$$

where m_H is the mass of the hydrogen atom and V_o is the orbital velocity of the particle. Assuming a corotating exosphere whose density is given by Eq. 1 and considering spherical particles of radius a (in centimeters) and density 1 cm^{-3}, we obtain approximate orbital decay rates of

$$dr/dt \simeq -5 \times 10^{-16}\, a^{-1}\, r^{1/2}\, e^{32.4/r} \qquad (3)$$

(in units of Uranus radii per year).

Numerical integration of Eq. 2 leads to the orbital lifetimes as a function of planetocentric distance and particle radius shown in Fig. 6. Orbital lifetimes are proportional to particle radius, and small particles will be selectively depleted. Such short orbital lifetimes have important implications for the population of small particles in the rings. The forces that confine the narrow, high optical depth, rings of Uranus are primarily gravitational. A strong nongravitational force will truncate the original size distribution of the rings at some minimum particle size, biasing the size distribution toward larger particles. An extended complex of tenuous rings, seen in the high phase angle ring images (*21*), indicates that a population of small (~1 μm) particles is present within the ring system. Given the lifetime (10^2 to 10^3 years) of such particles, this may represent a steady-state population of fine material derived from the rings or from shepherd satellites (or from both) and spiraling toward the planet.

A ring experiences a collective drag torque from the smallest particles remaining in the ring. The magnitude of this torque depends on the particle size distribution, which for the Uranian rings is not well known. However, estimates of decay time are possible for the α, β, and ϵ rings where surface mass densities and mean optical depths are known. If each ring is considered an isolated system (that is, disregarding the contribution of possible shepherd satellites), then the drag torque on a ring is proportional to the ratio of the weighted average of particle areas divided by the weighted average of particle masses. For each of these three rings

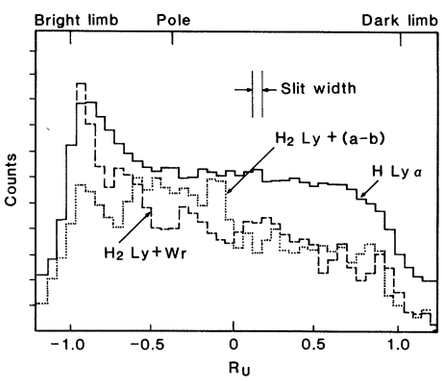

Fig. 4. Brightness profiles across the sunlit hemisphere of Uranus on 24 January 1986 U.T. H Lyman α, 1216 Å; H_2 Ly + Wr, 902 to 1115 Å; H_2 Ly + (*a*–*b*), 1273 to 1514 Å.

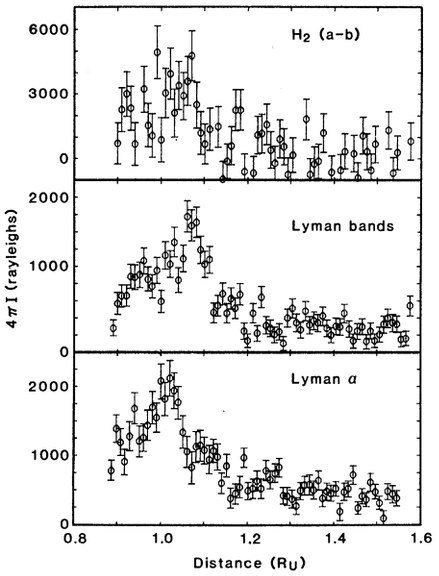

Fig. 5. Altitude profiles of H Lyman α and H_2 emission inferred from the limb drift at 2 hours before encounter. The UVS slit, which was tangent to the limb, drifted slowly through the atmosphere above the limb and onto the disk.

(assuming a single particle size), this can be approximated by $<\tau>/\Sigma$, where $<\tau>$ is the mean optical depth and Σ is the surface mass density of the ring. From the observed ring parameters (*22*), we obtain lifetimes of 4×10^6, 8×10^6, and 6×10^8 years for the α, β, and ε rings, respectively. Although orbital lifetimes would be increased by additional mass in ring shepherds or by a substantial population of large particles, lifetimes still would not be indefinite, and a recent origin of the rings should be considered.

It is legitimate to ask how confidently we can extrapolate the H number density at 1.2 R_U to the distance of the rings. Of the measured quantities, density and temperature, the latter contributes nearly all the uncertainty. The 750 K temperature is based on the fit in Fig. 1A rather than on the altitude difference between A and B. We estimate an uncertainty of ±100 K. The corresponding uncertainties in H number density and orbital lifetimes are shown in Fig. 6. The effect of the ring drag on the gas is negligible because nearly all the atoms are launched on ballistic trajectories from the exobase, with a free-fall time of 1 hour or less.

The aurora. From 2 days before to 2 days after encounter, the resolution of the UVS was sufficient to identify localized aurora. On the sunlit side recognition of aurora is hampered by the bright electroglow, but on the dark side auroral sources are clearly evident above the low-level H Lyman α emission. On at least eight occasions over a 25-hour period, auroral emission was observed from a region that rotated with the planet and is consistent with the location (*23*) of the south magnetic pole. High spatial resolution scans at 11 and 16 hours after encounter show a well-confined auroral region approximately 15° to 20° in diameter centered on the south magnetic pole. Assuming a circular auroral cap of uniform intensity with a diameter of 20° of latitude leads to intensities of 1.5 and 9 kRy for H Lyman α and H_2 band emissions. This corresponds to a total emitted power of 10^{10} W from the south magnetic pole and an input power of 10^{11} W. For an equatorial surface field strength of 0.23 G and a magnetosphere with little internal plasma pressure, the diameter of the polar cap is expected to be an ellipse approximately 15° by 25° for standard solar wind conditions. This expectation is in satisfactory agreement with our observation.

The auroral spectra resemble the "hot spot" aurora observed on Saturn (*8*). The spectra are characterized by emission of H_2 Rydberg bands and H Lyman α emission from vertical column abundances of H_2 of order 10^{20} cm^{-2}, requiring primary electrons approximately 10 keV in energy. The intensity ratio I(H Ly α): I(H_2 Ly + Wr) ~ 0.2 is the value expected for electron excitation of pure H_2. The energy deposition rates required for the production of the aurora are given in Table 2. The disk-averaged brightnesses of the auroral emissions are I(H_2 Ly + Wr) ~ 250 Ry and I(H Ly α) ~ 45 Ry, compared to observed values of dayside nonauroral emissions, I(H_2 Ly + *a–b*) ~ 1800 Ry and I(H Ly α) ~ 1500 Ry. The energy delivered in auroral precipitation is comparable to the input power of the electroglow process (Table 2).

Before the Voyager encounter, observations of bright H Lyman α emissions from Uranus by the International Ultraviolet Explorer (IUE) were interpreted as aurora (*24*). The H Lyman α emission brightness of 1500 Ry measured by Voyager near the subsolar point on Uranus is in fairly good agreement with the IUE time-averaged value of 1400 Ry, but this emission is due almost entirely to electroglow (*11*) and resonance scattering (*25*). The 45-Ry disk-averaged value of auroral H Lyman α emission means that the polar aurora is a minor source, even if there is an equivalent dayside aurora. The sporadic brightenings in H Lyman α emission recorded by IUE may represent changes in the brightness of the electroglow. Voyager observations show evidence for temporal variations of 50% in H_2 and H Lyman α electroglow emissions from Uranus within a few days, and the H Lyman α emission from Saturn changed between Voyager encounters (the change did not correlate with the solar H Lyman α flux). For the low electron temperature at Uranus, a temperature change of only 15% will lead to a 50% change in the H Lyman α intensity.

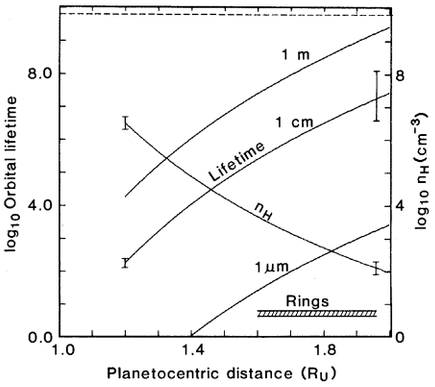

Fig. 6. Hydrogen number density and orbital lifetimes (in years) of particles of various sizes as a function of distance from the center of Uranus. The uncertainties in hydrogen density and orbital lifetimes corresponding to the ±100 K uncertainty in exospheric temperature are indicated by the error bars. The dashed line represents the age of the solar system.

Resonance emissions. Hydrogen Lyman α emissions from the sunlit atmosphere of Uranus arise from resonant scattering of H Lyman α from the interstellar medium (*25*) and the solar line and from particle excitation of H and H_2. If energetic protons or H atoms contribute to the electroglow, then H Lyman α photons are emitted from the exciting particles as well. The intensity of the resonantly scattered H Lyman α emission depends on the upper atmospheric temperature and on the H column abundance. The temperature has been determined from the stellar and solar occultation experiments, and the H density near the equator has been measured in the solar occultation. We expect the H density to be fairly uniform over the planet, because H from the asymmetric source will be efficiently redistributed through lateral flow in the exosphere. The time constant for lateral flow is several days, whereas the diffusive time constant may be several months to several years depending on the eddy diffusion coefficient. The efficiency of lateral flow implies that the global H distribution will be determined by the balance of ballistic fluxes at the exobase. Since the temperature appears to be uniform, the H density should also be uniform.

Initial analysis of data from the solar occultation experiment indicates a vertical H column abundance of 5×10^{16} cm^{-2}. At 750 K this column will reflect approximately 350 Ry from the interstellar medium and 150 Ry from the sun, for a total of 500 Ry. If most of the scattering occurs lower in the atmosphere where the temperature is about 120 K, the component from the interstellar medium will be unchanged, but the solar

component will be only 50 Ry, for a total of 400 Ry (*25*). The subsolar intensity is approximately 1500 Ry, so that the remaining 1 kRy must be collisionally excited.

The H Lyman α emission intensity from the nightside of Uranus, in the nonauroral regions, is at least 170 Ry and may be variable. Resonance scattering of emissions from the interstellar medium from a column abundance of 5×10^{16} cm^{-2} at 750 K will contribute only 100 Ry. A column abundance of 4×10^{17} cm^{-2} is required to produce 170 Ry. Such a large column abundance is unlikely, so that other excitation mechanisms such as radiative transfer from the dayside via the H corona and collisional excitation must be considered.

We have made a marginal detection of He 584 Å in resonance scattering of the solar line by helium in the Uranian atmosphere. With the UVS field filled by the sunlit hemisphere, a 10^5-second integration yields an intensity of 0.11 ± 0.08 Ry. This intensity corresponds to an eddy diffusion coefficient less than 3×10^7 cm^2 sec^{-1}.

Ultraviolet albedo of the atmosphere of Uranus. Longward of 1500 Å, the spectrum of Uranus is dominated by sunlight reflected by the atmosphere. Sunlight is scattered by both the gases and particulates, and its spectrum is modified by hydrocarbon absorption. Model calculations for Jupiter (*8*) fit spectra from both Jupiter and Saturn equally well at the resolution of the UVS (*10, 14*). Uranus has a higher far ultraviolet albedo than either Jupiter or Saturn and hence may be expected to show the effects of C_2H_2 in the gaseous as well as the condensed phase. We estimate that sunlight at 1490 Å penetrates to 0.5 to 1.0 mbar, through a vertical column abundance of C_2H_2 in the range 1×10^{17} to 3×10^{17} cm^{-2} with a mixing ratio of about 2×10^{-7} (*17*). In the model, sunlight at 1600 Å penetrates to 56 mbar through a column abundance of C_2H_2 less than 5×10^{17} cm^{-2}. Initial analysis indicates that condensation of C_2H_2 in the lower stratosphere may be required (*5*) to explain the spectrum, as was the case with the IUE spectra (*4*).

Other features. The spectrum of Uranus in Fig. 3 contains discrete emission features that correspond approximately to neutral carbon transitions at 1657, 1560, 1329, and 1280 Å. The estimated brightness of the feature at 1657 Å is about 50 Ry. A 1280-Å emission feature is also produced by Raman scattering of the solar H Lyman α line in H_2.

REFERENCES AND NOTES

1. In comparing the occultation light curves at various latitudes, we used an equilibrium figure for the planet that was calculated assuming GM = 5,793,920 km^3 sec^{-2} (G, universal gravitational constant; M mass), a rotation period of 17.3 hours, and $J_2 = 3.346 \times 10^{-6}$ and $J_4 = 3.21 \times 10^{-5}$.
2. In the analysis of these observations, we followed the procedure established by G. R. Smith *et al.*, *J. Geophys. Res.* **88**, 8667 (1983).
3. B. D. Savage *et al.*, *Astrophys. J.* **216**, 291 (1977).
4. Th. Encrenaz *et al.*, *Astron. Astrophys.*, in press.
5. S. K. Atreya, in *Uranus and Neptune*, J. T. Bergstralh, Ed. (*NASA Conf. Publ.* **2330**, 1984), p. 55.
6. R. G. French *et al.*, *Icarus* **53**, 399 (1983).
7. A. L. Broadfoot *et al.*, *Science* **204**, 979 (1979).
8. B. R. Sandel *et al.*, *ibid.* **215**, 548 (1982).
9. G. R. Smith *et al.*, *J. Geophys. Res.* **88**, 8667 (1983).
10. D. E. Shemansky, *ibid.* **90**, 2673 (1985).
11. ——— and G. R. Smith, *Geophys. Res. Lett.* **13**, 2 (1986).
12. D. M. Hunten *et al.*, in *Saturn*, T. Gehrels and M. S. Matthews, Eds. (Univ. of Arizona Press, Tucson, 1984), p. 671.
13. Several aspects of the H_2 models depend on recent unpublished work by A. J. Ajello, D. E. Shemansky, Y. L. Yung, A. Dalgarno, S. Guberman, T. L. Kwok, and A. Posen (1986).
14. D. E. Shemansky and J. M. Ajello, *J. Geophys. Res.* **88**, 459 (1983).
15. The energy distribution of the exciting electrons should be nearly Maxwellian because electron-electron relaxation is rapid; this distribution was used for our calculated spectra. The threshold for excitation of the H_2 emissions is about 10 eV, so that the excitation in this model is caused by electrons in the high-energy tail of the Maxwellian distribution. These electrons also dissociate H_2 and heat the atmosphere. The ratio of the H production rate to the ionization rate, which depends on the electron temperature, is ten times higher at Uranus than at Saturn. The total rates of production of escaping H are comparable at Uranus and Saturn.
16. The H_2 column abundance is inferred from self-absorption in the spectrum.
17. D. E. Shemansky, D. F. Strobel, Y. L. Yung, in preparation.
18. J. H. Waite *et al.*, *J. Geophys. Res.* **88**, 6143 (1983).
19. R. V. Yelle, B. R. Sandel, D. E. Shemansky, S. Kumar, *J. Geophys. Res.*, in press.
20. K. M. Hagenbuch and R. E. Hartle, *Phys. Fluids* **12**, 1551 (1969).
21. B. A. Smith *et al.*, *Science* **233**, 43 (1986).
22. R. G. French, J. L. Elliott, S. E. Levine, *Icarus*, in press.
23. N. F. Ness *et al.*, *Science* **233**, 85 (1986).
24. J. T. Clarke *et al.*, *J. Geophys. Res.*, in press.
25. R. V. Yelle and B. R. Sandel, *Geophys. Res. Lett.* **13**, 89 (1986).

26. We thank R. S. Polidan, J. T. Clarke, and J. H. Waite for helpful discussions and the Voyager Project personnel at the Jet Propulsion Laboratory for the enthusiastic efforts that have made this mission successful. Supported by the Jet Propulsion Laboratory, California Institute of Technology, under NASA contract NAS 7-100. Additional support was provided by the Planetary Sciences Discipline of NASA's Office of Space Sciences under contracts NAGW-610, NSG-7404, and NAGW-649.

28 March 1986; accepted 5 May 1986

Voyager 2 Radio Science Observations of the Uranian System: Atmosphere, Rings, and Satellites

G. L. Tyler, D. N. Sweetnam, J. D. Anderson, J. K. Campbell, V. R. Eshleman, D. P. Hinson, G. S. Levy, G. F. Lindal, E. A. Marouf, R. A. Simpson

Voyager 2 radio occultation measurements of the Uranian atmosphere were obtained between 2 and 7 degrees south latitude. Initial atmospheric temperature profiles extend from pressures of 10 to 900 millibars over a height range of about 100 kilometers. Comparison of radio and infrared results yields mole fractions near the tropopause of 0.85 and 0.15 ± 0.05 for molecular hydrogen and helium, respectively, if no other components are present; for this composition the tropopause is at about 52 kelvins and 110 millibars. Distinctive features in the signal intensity measurements for pressures above 900 millibars strongly favor model atmospheres that include a cloud deck of methane ice. Modeling of the intensity measurements for the cloud region and below indicates that the cloud base is near 1,300 millibars and 81 kelvins and yields an initial methane mole fraction of about 0.02 for the deep atmosphere. Scintillations in signal intensity indicate small-scale structure throughout the stratosphere and upper troposphere. As judged from data obtained during occultation ingress, the ionosphere consists of a multilayer structure that includes two distinct layers at 2,000 and 3,500 kilometers above the 100-millibar level and an extended topside that may reach altitudes of 10,000 kilometers or more. Occultation measurements of the nine previously known rings at wavelengths of 3.6 and 13 centimeters show characteristic values of optical depth between about 0.8 and 8; the maximum value occurs in the outer region of the ε ring, near its periapsis. Forward-scattered signals from this ring have properties that differ from those of any of Saturn's rings, and they are inconsistent with a discrete scattering object or local (three-dimensional) assemblies of orbiting objects. These signals suggest a new kind of planetary ring feature characterized by highly ordered cylindrical substructures of radial scale on the order of meters and azimuthal scale of kilometers or more. From radio data alone the mass of the Uranian system is GM_{sys} = 5,794,547 ± 60 cubic kilometers per square second; from a combination of radio and optical navigation data the mass of Uranus alone is GM_U = 5,793,939 ± 60 cubic kilometers per square second. From all available Voyager data, including imaging radii, the mean uncompressed density of the five major satellites is 1.40 ± 0.07 grams per cubic centimeter; this value is consistent with a solar mix of material and apparently rules out a cometary origin of the satellites.